B.A.R.C.-318

INDC(IND)-005/G

R/630

Data Requested
28 May 68
30 Sep 68

B.A.R.C.-318

'सत्यमेव जयते'

GOVERNMENT OF INDIA
ATOMIC ENERGY COMMISSION

30093

ANGULAR ANISOTROPY OF FISSION FRAGMENTS IN TERNARY FISSION OF U^{235} INDUCED BY 3—MEV NEUTRONS

by

D. M. Nadkarni
Nuclear Physics Division

BHABHA ATOMIC RESEARCH CENTRE
BOMBAY, INDIA
1967

B.A.R.C.-318

B.A.R.C.-318

GOVERNMENT OF INDIA
ATOMIC ENERGY COMMISSION

ANGULAR ANISOTROPY OF FISSION FRAGMENTS IN TERNARY FISSION OF U^{235} INDUCED BY 3-MEV NEUTRONS

by

D.M. Nadkarni
Nuclear Physics Division

BHABHA ATOMIC RESEARCH CENTRE
BOMBAY, INDIA
1967

ABSTRACT

The values of angular anisotropy of fragments in binary and ternary fission of U^{235} induced by 3 MeV neutrons have been determined with two independent methods. In the first method fission fragments and long range alpha particles were detected with a gridded ionization chamber and a CsI crystal respectively and in the second method semi-conductor detectors were used to detect fission fragments and long range alpha particles. The values of $\left[N(0^o)/N(90^o)\right]$ for cases of binary and ternary fissions are found to be different. The probability for emission of long range alpha particles in 3 MeV neutron induced fission is found to be lower than that in thermal neutron induced fission. A decrease in the average single fragment kinetic energy of ternary fragments compared to that of binary fragments is observed in 3 MeV neutron induced fission similar to that in thermal neutron fission. It is shown that on the basis of the angular distribution of long range alpha particles and ternary fragments it is possible to learn at what stage in the fission process the long range alpha particles are emitted.

ANGULAR ANISOTROPY OF FISSION FRAGMENTS IN TERNARY FISSION OF U^{235} INDUCED BY 3-MeV NEUTRONS

by

D. M. Nadkarni

1. INTRODUCTION

Emission of light charged particles in nuclear fission occurs with a very low probability[1] and in over 90 percent fission events accompanied by these particles (ternary fission events) the light charged particles are long range alpha particles[2] (LRA). These LRA are known to be preferentially emitted perpendicular to the direction of motion of fission fragments indicating that these are emitted close to the scission stage. Therefore, LRA can serve as a probe to investigate the properties of highly elongated nuclear configuration. The study of the various aspects of ternary fission such as (i) the angular distribution of LRA and ternary fission fragments with respect to the incident projectile direction, (ii) the probability of LRA emission, and (iii) the energy spectrum of LRA and ternary fission fragments and the dependence of (i), (ii) and (iii) on the excitation energy of the fissioning nucleus can be helpful in understanding the ternary fission mechanism, which is not clearly understood at present.

The angular distributions of binary and ternary fission fragments can provide information on the angular momentum distributions (K-distributions) in the fissioning nucleus undergoing binary and ternary fission. The angular distributions of binary fission fragments have been generally found to be 0^{o}-peaked when the excitation energy is well above the fission threshold. The angular distribution of ternary fission fragments was first measured by Ramanna et al[3] in the 14 MeV neutron induced fission of U^{238} using emulsion technique and a 90^{o}-peaked angular distribution was indicated. Subsequent measurements for the same case by Gillet et al[4] also using the emulsion technique indicated very small anisotropy. However, in 17.5 MeV proton induced fission of U^{238}, Atneosen et al[5] observed that the ternary fission fragments have nearly the same 0^{o}-peaked angular distribution as the binary fission fragments. Therefore an uncertainty exists at present about the nature of fragment angular distributions in ternary fission which could be partly due to the large statistical errors arising from the low probability of such events. Also at these incident energies there is a substantial contribution (> 50%) from second and third chance fissions and consequently the observed angular distribution is a resultant of angular distributions of a number of nuclides fissioning at different excitation energies. With a view to clarify the situation, the angular anisotropies $[N(0^{o})/N(90^{o})]$ of binary and ternary fission fragments in the 3 MeV neutron induced fission of U^{235} have been determined with two different methods in the present work. This neutron energy was chosen because at this energy only first chance fissions contribute so that the fissioning nucleus is specified and also to correlate the results of the present work with the measured[6] anisotropy of LRA at the same neutron energy. In the present measurements the relative LRA emission probability in 3 MeV and thermal neutron induced fission of U^{235} have also been determined.

The angular anisotropy of binary and ternary fission fragments were determined with two independent methods. In the first method a gridded ionization chamber was used to measure the direction of emission of fission fragments and CsI(Tl) crystal for detecting

LRA and in the second method semi-conductor detectors where used for detecting both fission fragments and LRA. The 3 MeV neutrons were generated with the $T(p,n) He^3$ reaction using a 5.5 MeV Van-de-Graaff Accelerator.

2. II. EXPERIMENTAL METHODS AND RESULTS

(a) Measurements With the Gridded Ionization Chamber-CsI(Tl) Crystal Set-up

(i) Principle of the Method: With gridded ionization chamber various methods have been used to measure the angles with respect to the electric field direction of the tracks of havily ionizing particles such as fission fragments. The method(7-9) used in the present work makes use of the fact that the amplitude V_g of the grid pulse varies linearly with the cosine of the angle θ which the fission fragment makes with the electric field direction. The grid pulse height V_g is given by

$$V_g = \frac{Qo}{C_g} \left(1-R^* \cos \theta / d_{cG}\right),$$

where Qo is the total charge of the electrons collected, C_g is the capacity of the grid and R^* is a quantity which depends only on the range of the fission fragment track. By making the incident neutron direction to coincide with the electric field direction, the angular distribution of fission fragments of a fixed energy or range can therefore be determined from the grid pulse height distribution(GPHD). The calibration of grid pulse heights into angles was determined using the isotropic angular distribution of the fragments in thermal neutron fission of U^{235}.

(ii) Experimental Arrangement

Fig (1) shows a schematic diagram of the experimental set-up used. The distances between the collector (Co) and the grid (G) and between the grid and the cathode (C) of the ionization chamber (A) were 0.7 cms and 2.1 cms respectively. A fissile source of U^{235} of about 1.5 cm^2 area and 1 mg/cm^2 thickness coated on 10 mg/cm^2 aluminium backing was mounted on the cathode. The source was prepared by the electroplating method. This thickness of aluminium backing was chosen to ensure that all natural alpha particles and fission fragments are stopped in the backing and only the LRA pass through. The LRA were detected by a CsI(Tl) crystal of 5 cms diameter and 0.5 mms thick mounted on a photomultiplier tube. This thickness of CsI(Tl) crystal is sufficient to stop LRA of energy upto 30 MeV. The CsI-crystal was placed close to the foil within about 0.2 cms to detect LRA in almost 2π solid angle. The chamber was filled to a pressure of about 114 cms of Hg, with pure argon gas which was purified at regular intervals during the experiments. The pulses from the grid and anode were fed to two pre-amplifier - amplifier systems with time constants optimized for best resolution. Neutrons of maximum energy 3.2 MeV were produced using $T(p,n)He^3$ reaction. The spread of the neutron energy as calculated from the thickness of the tritium target was about 200 KeV. The neutron flux at the fissile target was estimated to be about 10^5 $n/cm^2/sec$. and the divergence of the neutron beam to be 3°.

The calibration of collector pulse heights in to fragment kinetic energies was done using the known energies of the light and

and heavy fragment peaks. For the purpose of this calibration, a thin foil of U^{235} of about 100 $\mu gm/cm^2$ was used. The region of collector pulse heights selected in the measurement with the thick foil corresponded to fragment kinetic energies of 70 to 110 MeV. The bias setting in the LRA-channel was such that LRA having energies greater than 10 MeV before energy loss in the aluminium backing could produce a gate for coincidence with the grid pulses. The GPHD for binary and ternary fission fragments for the selected energy region were recorded in anti-coincidence and coincidence with these gate pulses using two 100-channel analysers. During the measurements the fission fragment and the LRA pulses were monitored. The count rates in 3 MeV neutron induced binary and ternary fission were about 100 per minute and 3 per hour respectively. The ratio of chance to true coincidences was found to be less than 0.2%. For the case of 3 MeV neutron induced fission, the data were recorded in 15 separate binary and ternary runs for a total duration of about 216 hours and a total of 559 ternary events were recorded. In the thermal neutron calibration runs made with the reactor Apsara about 2579 ternary events were recorded. The GPHD for fission induced by thermal and 3 MeV neutrons are shown in Figs. 2 and 3 respectively.

(iii) Treatment of Experimental Data

The observed deviation of the measured GPHD in thermal neutron fission from the rectangular distribution can be attributed mainly to the following factors:
(a) the thickness of the U^{235} target foil, which results in a reduction of counts at larger angles and (b) the relatively large width of the

fragment energy region selected. As a result the complete angular distribution of binary and ternary fission fragments could not be obtained uniquely from the measured distributions. However the GPHD for binary fission fragments in thermal neutron fission was analysed by dividing the selected energy region into five intervals each interval giving a rectangular distribution with an area proportional to the yield corresponding to that energy interval. The superposition of these distributions was found to give a fairly good fit to the observed GPHD. (Fig.2). From this analysis channel widths of equal solid angles in the 0° and 90° region corresponding to average angles $\theta_1 = 7^{\circ}$ and $\theta_2 = 85^{\circ}$ were determined such that it gives isotropy for the case of thermal neutron binary fission. On this basis the ratio $N(7^{\circ})/N(85^{\circ})$ as obtained from the GPHD for the thermal neutron ternary fission was found to be (0.75 ± 0.08). In the case of thermal neutron ternary fission a value of this ratio less than unity is expected as a result of a preferential detection of ternary fragments at 90° due to a finite separation of LRA detector from the foil and the LRA-fragment angular correlation. This ratio in thermal neutron induced ternary fission was used to correct the angular anisotropy in ternary fission for the above mentioned effect.

The very low counting rates in 3 MeV neutron induced ternary fission necessitated choosing wider angular widths (full width $\sim 30^{\circ}$) to determine angular anisotropy. At these angles equal solid angular widths were determined by thermal neutron induced fission runs by surronding the chamber with paraffin blocks. The observed angular anisotropy and that corrected for the preferential detection of ternary fragments at 90^{o} in the 3 MeV neutron fission are given in Table I.

(b) Measurements With Semiconductor Detectors

(i) Experimental Set-up, Electronics and Procedure

A schematic diagram of the experimental set-up is shown in Fig. (4). A semi-conductor detector D1 of 200 mm^2 area was placed close to the aluminium backing of the U^{235} foil and was operated at 150V to detect LRA of energies upto 25 MeV. Two identical detectors D2 and D3 each having an active area of 100 mm^2 and operated at 60V were used to detect fission fragments emitted along and at right angles to the incident neutron beam direction by mounting these symmetrically at a distance of 1.2 cms from the target foil. The very low ternary fission cross-section necessitated keeping the detectors at such short distances. The U^{235} foil used in these measurements was the same as the one used in the ionization chamber method.

The pulse outputs from the three detectors were amplified with low-noise charge sensitive pre-amplifier amplifier systems and the pulse height distributions from 0^{o} - and 90^{o}-detectors were simultaneously recorded in coincidence and anti-coincidence with the LRA pulses in the four quadrants of a TMC-400 channel analyser. The counts from D1, D2 and D3 detectors were monitored during the measurements. The relative solid angles of 0^{o}-and 90^{o}-detectors were determined by carrying out thermal fission runs by surrounding the chamber on all sides with 12" thick paraffin blocks. During the experiment with 3 MeV neutrons the fission chamber was covered with Cd sheets to eliminate any thermal neutron background.

In the first set of measurements the distance between the neutron source and the fissile foil was 20 cms corresponding to a divergence of about 2^{o} in the incident-neutron beam direction. The fission count rate in each of the 0^{o}-and 90^{o}-detectors was about 20 per minute and the coincident count rate for the ternary fission fragments was extremely low, about 0.7 per hour on an average. A total of 4.5×10^{5} binary events and 193 ternary events in 3 MeV neutron induced fission were recorded in a series of separate runs for a duration of nearly 119 hours. This set of measurement was used only to determine the anisotropy of the binary fission fragments since the statistical accuracy for the ternary fragments was extremely poor.

The second set of measurements were aimed at obtaining ternary data with better statistical accuracy which necessitated keeping a shorter distance of 7 cms between the neutron source and the fission target. In this case the neutron flux at the fissile target was estimated to be $\sim 10^{6} n/cm^{2}/sec.$ and the divergence of the incident neutron beam to be $\sim 6^{o}$. The binary count rates in each of the 0^{o}-and 90^{o}-detectors was about 180 per minute and the fragment-LRA coincidence count rate was about 4 per hour. About 3×10^{6} binary and 810 ternary events were recorded in this run for 3 MeV neutron fission. Thermal neutron fission runs were carried out in between fast neutron runs to determine relative soild angles and in these thermal runs about 3.5×10^{6} binary and 1590 ternary fission events were recorded. The chance coincidence rate was determined by appropriately delaying the pulses in the LRA channel and was found to be less than 1 percent of the true coincidence rate. The fragment pulse height distribution in the 0^{o}- and 90^{o}- detectors in 3 MeV and thermal neutron induced binary and ternary fissions are shown in Figs. 6 to 9.

(ii) Experimental Results

Fission Fragment Anisotropy

The measured values of $[N(0^{o})/N(90^{o})]$ for binary and ternary fission in 3 MeV and thermal neutron induced fission are given in Table I. These measured values corrected for the effects of geometrical resolutions and non-uniformity of fast neutron flux across the fissile target are also given in the Table I. These corrections were evaluated by simulating these measurements in the computer CDC-3600. Using the experimental geometry, Monte Carlo calculations were made to compute the ratio $[N(0^{o})/N(90^{o})]$ for the binary case taking into account the non-uniform neutron flux across the foil and assuming the fragment angular distribution of the type:

$$N(\theta) \propto (1 + b \cos^2 \theta) \qquad \ldots\ldots\ldots\ldots\ldots\ldots(2)$$

with b as a variable parameter. In the case of ternary fission first the ratio $[N(0^{o})/N(90^{o})]$ of the ternary fragments detected at 0^{o} and 90^{o} was computed assuming isotropic fragment distribution to determine the biasing of the data due to the LRA-fragment correlation, since the LRA were not detected exactly in 2π solid angle. In this computation known(1,5), LRA-fragment angular corrleation was used and the computed ratio $[N(0^{o})/N(90^{o})]$ was found to depend sensitively on the position of the centre of mass of the target foil relative to the centre of the LRA detector. It was found necessary to change this distance between centres of foil and LRA by about 0.1 cms to obtain agreement between the computed ratio and the measured ratio for the thermal neutron induced ternary fission. The geometry thus fixed was then used to compute the ratio $[N(0^{o})/N(90^{o})]$ for the ternary fragments taking into account the fast neutron flux variation over the foil. In these computations it was assumed that the LRA-fragment angular correlation in 3MeV and thermal neutron induced fission are similar. The angular distribution of ternary fragments was taken to be the same as given by Eq. (2) with b as a variable parameter. The values of b giving best agreement of computed $[N(0^{o})/N(90^{o})]$ ratios with that observed in the 3 MeV neutron induced binary and ternary fissions were obtained. The corrected values of $[N(0^{o})/N(90^{o})]$ given in Table I correspond to these values of b.

Binary to Ternary Ratio

By comparing the binary and ternary counting rates the observed binary to ternary ratios in 3 MeV neutron fission as compared to that in thermal neutron fission were found to be (1.41 $\pm$ 0.11) and (1.24 $\pm$ 0.08) for sission fragments detected in 0^{o}- and 90^{o}-detectors respectively. The absolute values of binary to ternary ratios in 3 MeV and thermal neutron induced fission were found to be very sensitive to the solid angles estimated and therefore only the relative values are given here.

Average Kinetic Energy of Fission Fragments

The pulse height distribution of fission fragments in 0^{o}- and 90^{o} detectors in thermal neutron binary fission were converted into energy distribution by using the kinetic energy data obtained by the time of flight method[10]. Using this calibration the average single fragment kinetic energy in thermal neutron induced ternary fission and 3 MeV neutron induced binary and ternary fission were calculated.

The decrease in the average kinetic energy of fission fragments in ternary fission compared to that in binary fission is $(\bar{E}_{KB} - \bar{E}_{KT})$ = 14.0± 3.2 MeV in 3 MeV neutron fission and (13.4 ± 2.1 MeV) in thermal neutron fission. These are uncorrected for the effects of detector response due to radiation damage and for the effect due to the fact that the hemisphere containing the light ternary fragment has higher yield of LRA than the hemisphere containing the heavy ternary fragment. However in a comparison of relative change in average kinetic energy of ternary and binary fission fragments in 3 MeV and thermal neutron fission the errors introduced by these effects are not significant.

III. DISCUSSION

(a) Angular Anisctropy

(i) Binary Fission

The angular anisotropy of the binary fission fragments observed in the ionization chamber method and semi-conductor detector method (set I), where nearly the same angular resolutions are involved, are found to be consistent within the experimental errors. The value of the anisotropy of binary fragments in each set of measurements as obtained with the semi-conductor detectors, after correction for the geometrical effects, is found to be 1.17 ± 0.02, in agreement with the earlier measurements of Simmons and Henkel[11] and Nesterov et al[12]. The anisotropy determined in the present work is consistent with the angular distribution of binary fission fragments of the type[11] $N(\theta) \propto (1 + .17 \cos^2\theta)$.

The angular distribution of fission fragments in neutron induced binary fission can be understood on the basis of Bohr's model[13] and its subsequent developments in which the assumption is made that the projection of the angular momentum ($\bar{I}$) on the fission axis (K) is not altered after the saddle point is passed and further the distribution function for K is a gaussian:

$$P(K) \propto \exp [-K^2/2 K_o^2], \text{ where } K_o^2 = \frac{J_{eff} T}{\hbar^2}$$

Here the effective moment of inertia J_{eff} and temperature T are evaluated at the saddle point. The predicted angular distribution of binary fission fragments is generally 0°-peaked when the excitation energy is well above the fission threshold because the distribution P(K) has a maxima at K equal to zero. The fragment anisotropy mainly depends on Ko^2 and the mean square angular momentum ($\overline{I^2}$). The anisotropy for the 3 MeV neutron fission of U^{235} on the basis of the relation between Ko^2 and the excitation energy given by Simmons and Henkel[11] is 1.156 which is in agreement with the present result within the experimental errors.

(ii) Ternary Fission

The value of the ratio $[N(0^o)/N(90^o)]$ for ternary fragments was found to be 0.89 ± 0.10 which is significantly lower than that of binary fragments showing that the angular distributions of binary and ternary fragments are different. The 90°-peaking of the angular distribution of ternary fragments indicated by the anisotropy observed in the present work is of very small magnitude compared to that reported in the case of 14 MeV neutron fission of U^{238} (3). The data reported by Gillet et al[4] for the case of 14 MeV neutron induced fission of uranium indicates almost isotropic angular distribution of ternary fragments within the large statistical errors. In the case of 17.5 MeV proton induced fission of U^{238}, Atneosen et al did not observe a decrease in the value of ternary fragment anisotropy compared to that for binary fragments. The different trend of binary and ternary fragment anisotropies in the present work and in the 17.5 MeV proton fission of U^{238} (5) is difficult to understand on the basis of the same mechanism of LRA emission in the two cases even though the fissioning systems involved in the two cases have different (Z,M), excitation energies and angular momenta and exhibit opposite variation of LRA emission probability with excitation energy.

It is of interest to correlate the anisotropy of ternary fission fragments determined in the present work with the anisotropy of LRA with respect to the incident neutron direction in 3 MeV neutron fission of U^{235} (6). It can be shown that if a particle a is emitted having an angular distribution with respect to a space-fixed axis, given by

$$N_a(\theta) \propto (1 + \alpha \cos^2 \theta) \qquad \ldots\ldots\ldots\ldots\ldots(3)$$

then the angular distribution of a second particle b emitted thereafter at right angles to a is given by

$$N_b(\theta) \propto (1 + \frac{\alpha}{2} \sin^2\theta) \qquad \ldots\ldots\ldots\ldots(4)$$

If it is assumed that the angular distribution of ternary fragments is the same as that of binary fragments, viz. $N(\theta) \propto (1 + .17 \cos^2 \theta)$, then on the basis of Exp. (3) and (4) the angular distribution of the LRA emitted thereafter is expected to be given by $N(\theta) \propto (1 + 0.085 \sin^2 \theta)$ giving a value of $[N(0^\circ)/N(90^\circ)]$ equal to 0.92. This is not in agreement with the experimentally observed LRA angular distribution, where 90°-peaking was not observed(3-6). On the other hand, if the angular distribution of LRA is given by $N(\theta) \propto (1 + \alpha \cos^2\theta)$ with $\alpha = 0.32 \pm 0.12$(3), then the resulting angular distribution of ternary fragments is expected to be of the type $N(\theta) \propto (1 - \beta \cos^2\theta)$

where $\beta = (0.14 \pm 0.05)$ if the LRA- fragment angular correlation is approximated by a delta function at 90°; and

$= 0.10 + 0.05$ if the LRA-fragment angular correlation is assumed to be the same as that observed(14) in thermal neutron induced fission of U^{235}. The value of $[N(0^{\circ})/N(90^{\circ})]$ for ternary fragments expected on this basis is between 0.86 to 0.90 which is consistent with the value determined in the present work.

On the basis of the above consideration it seems that either the angular distribution of ternary fragments is intrinsically different from that of binary fragments or though the intrinsic angular distributions are the same due to the restrictions imposed by the LRA angular distribution, the ternary fragment angular distribution is observed to be different from that of binary fragments. However, on the basis of the first possibility that the ternary fragment angular distribution corresponds to that observed in the present work, the resultant LRA anisotropy using Exps. (3) and (4), is expected to be 1.05 which is small compared to that observed. Hence it appears that the LRA are emitted earlier in the process with a 0°-peaked angular distribution and since these LRA are also constained to be emitted preferentially at right angles to the fission axis, this results in the 90° peaking of the angular distribution of ternary fragments.

Different angular distributions of binary and ternary fragments can be expected on the basis of Bohr's Model due to the following possibilities:

1. The intrinsic distribution function for K at saddle point can be different for cases leading to binary and ternary fission. This can come about if LRA emission is associated with certain specific saddle point configurations.

2. Even if the distribution function for K in both the cases is identical, LRA emission probability can depend on the orientation of fission axis with respect to incident neutron direction or on the value of K[3]. The present results indicate a preferential emission of LRA for higher values of K.

3. A difference in angular distributions of binary and ternary fragments can also come about if the assumed constancy of quantum number K after saddle stage is not valid in the cases leading to the emission of LRA at some stage before scission.

The first possibility predicts an LRA anisotropy small compared to that observed and the second and third possibilities, though consistent with the observed LRA and ternary fragment anisotropy, are experimentally indistinguishable. The models of ternary mechanisms[15,16] according to which LRA is a post-scission phenomenon and occurs from separated fission fragments do not seem to explicitly predict different binary and ternary fragment angular distributions.

(b) Binary to Ternary Ratio

The binary to ternary ratio in 3 MeV neutron fission of U^{235} has been observed to be higher than that in thermal neutron fission, the increase being 41 ± 11% and 24 ± 8% for fission fragments emitted along and at right angles to the incident neutron beam. This is to be compared with the 20% increase in binary to ternary ratio observed[6] where fission fragments emitted at all angles were detected. These results are in agreement with the general decrease[1] in LRA emission probability with increase in incident neutron energy upto 14 MeV.

Coleman et al[17] and more recently Thomas and Whetstone[18] have observed an increase in LRA emission probability with increase in incident charged particle energy. The reason for this entirely different variation of LRA emission probability with excitation energy in neutron and charged particle induced fission is not known. The decrease of LRA emission probability in neutron induced fission has been qualitatively attributed to various effects such as the effects of increasing angular momentum[19], competition of LRA and pre-scission neutron emission[6], decrease in α-cluster probability[17] with excitation energy. The increase in LRA emission probability with excitation in charged particle induced fission has been mainly ascribed[17] to the higher probability of LRA emission from symmetric fission events than from asymmetric fission events. On the basis of this assumption and the observed variation of fragment anisotropy with mass asymmetry[20] a dependence of LRA emission probability on the angle of emission of fragment is expected. It is possible that the different variation of LRA emission probability with excitation energy and the different ternary fragment anisotropy observed in neutron and proton induced fission are correlated.

(c) Average Kinetic Energy of Fission Fragments

It has been observed[21,22] that in thermal neutron fission of U^{235} the average kinetic energies $\bar{E}_{KB}$, $\bar{E}_{KT}$ and $\bar{E}_{\alpha}$ of binary, ternary fragments and LRA respectively are related by: $\bar{E}_{KB} = \bar{E}_{KT} + \bar{E}_{\alpha}$. From this it can be estimated that the average separation of fragment charge centres at scission in ternary fission is larger by about 5 to 6% compared to that in binary fission, indicating that the LRA are emitted from a more stretched scission configuration.

In the present work ($\bar{E}_{KB}$ - $\bar{E}_{KT}$) was observed to be 14.0 + 3.2 MeV and 13.4 ± 2.1 MeV in 3 MeV and thermal neutron fission of U^{235} respectively. The average energy of LRA in 3 MeV and thermal induced fission of U^{235} was found (6) to be 15.3 ± 0.4 MeV and 15.1 ± 0.2 MeV respectively. Hence a similar relationship as above between the average single fragment kinetic energy of binary and ternary fragments and LRA is found to hold approximately in the case of 3 MeV neutron fission of U^{235}. Therefore, in so far as the average kinetic energy of fragments can be used to compare the scission configurations in the two cases, this supports the view that in the case of 3 MeV neutron fission also the distance between the fragment charge centres at scission in ternary fission is more by about 5 to 6% than in binary fission.

ACKNOWLEDGEMENTS

I am very much indebted to Dr. R. Ramanna for his guidance and many helpful discussions. I am thankful to Dr. S.S. Kapoor for helpful discussions, to Messrs P.N. Rama Rao, S.R.S. Murthy and B.R. Ballal for their help in carrying out the experiment. and to Mr.S.K. Kataria for his help with the computer calculations.

TABLE I

SUMMARY OF ANGULAR ANISOTROPY RESULTS

	BINARY FISSION			TERNARY FISSION		
	Thermal Neutron Induced	3 MeV Neutron Induced: Observed	3 MeV Neutron Induced: Corrected	Thermal Neutron Induced	3 MeV Neutron Induced: Observed	3 MeV Neutron Induced: Corrected
$\frac{N(17^\circ)}{N(81^\circ)}$ With ionization chamber and CsI set up	1.00[a]	1.08±0.03	-	0.75±0.08	0.64±0.07	0.85±0.12[b]
$\frac{N(0^\circ)}{N(90^\circ)}$ With semiconductor detectors	0.99±0.01	1.11±0.01[c] (Set I) 1.04±0.01[c] (Set II)	1.17±0.02[d] (Set I and II)	0.74±0.04	0.65±0.05	0.89±0.10[d]

a. The isotropy here is used to obtain equal solid angle widths

b. Corrected for the preferential detection of ternary fragments at 90°, using thermal neutron fission data (uncorrected for angular resolution effects).

c. The lower value of observed ratio for set II is due to the non-uniform fast neutron flux across the target foil.

d. Corrected for the effects of non-uniform neutron flux and finite angular resolution (see text).

APPENDIX

Angular Distribution of Particles a and b emitted successively at right angles to each other

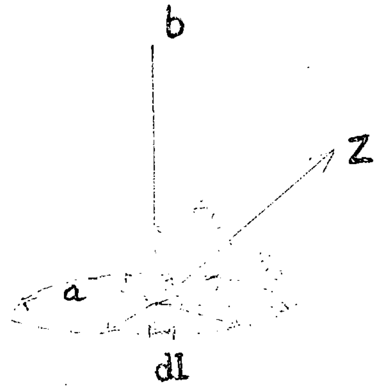

Let the angular distribution with respect to Z-axis of a particle a be given by

$$N(\phi_a, \phi_a) \propto (1 + \alpha \cos^2 \theta) \qquad (1)$$

and a particle b be then emitted at right angles to the direction of emission of a, with equal probability in 2π radians. Then

$$N(\theta_b, \phi_b)\, d\Omega_b = \oint N(\theta_a, \phi_a)\, d\Omega_b\, dl \qquad (2)$$

where $d\Omega_b$ is an element of solid angle and dl is an element of length on a circle of unit radius given by

$$dl^2 = d\,\theta_a^2 + \sin^2\theta_a\, d\phi_a^2$$

Thus, $N(\theta_b, \phi_b) = \int N(\theta_a, \phi_a) d\theta_a \sqrt{1 + \sin^2\theta_a \left(\frac{d\phi_a}{d\theta_a}\right)^2} \qquad (3)$

Now, the condition of perpendicularity of a and b gives,

$$\cos\theta_a \cos\theta_b + \sin\theta_a \sin\theta_b \cos(\phi_a - \phi_b) = 0 \qquad (4)$$

From Exp (4) it follows that

$$\cos(\phi_a - \phi_b) = -\frac{\cos\theta_b \cos\theta_a}{\sin\theta_b \sin\theta_a} \qquad (5)$$

and by differentiating Exp (4)

$$\frac{d\phi_a}{d\theta_a} = \frac{\text{Sin}\theta_b \cos\theta_a \cos(\phi_a-\phi_b) - \text{Cos}\theta_b \,\text{Sin}\theta_a}{\text{Sin}\theta_b \,\text{Sin}\theta_a \,\text{Sin}(\phi_a-\phi_b)}$$

$$= \frac{-\text{Cos}\theta_b \,\text{Cosec}\ \theta_a}{\sqrt{-\angle\text{Cos}(\theta_b-\theta_a)\text{Cos}(\theta_b+\theta_a)}} \qquad (6)$$

Using Exp(5)

Now, substituting Exp (6) in Exp (3) and simplifying

$$N(\theta_b,\phi_b) = \int_{\pi/2 - \theta_b}^{\pi/2 + \theta_b} N(\theta_a,\phi_a)\sqrt{\frac{\text{Sin}^2\theta_a}{\text{Sin}^2\theta_a-\text{Cos}^2\theta_b}}\ d\theta_a$$

$$= \int_{\pi/2 - \theta_b}^{\pi/2 + \theta_b} (1 + \alpha\text{Cos}^2\theta_a)\sqrt{\frac{\text{Sin}^2\theta_a}{\text{Sin}^2\theta-\text{Cos}^2\theta_b}}\ d\theta_a$$

Substituting $x=\cos\theta_a$ in this and simplifying

$$N(\theta_b,\phi_b) = \int_{-\text{Sin}\theta_b}^{\text{Sin}\theta_b} \frac{dx}{\sqrt{\text{Sin}^2\theta_b-x^2}} + \alpha\int_{-\text{Sin}\theta_b}^{\text{Sin}\theta_b} \frac{x^2dx}{\text{Sin}^2\theta_b-x^2}$$

$$= \left[\text{Sin}^{-1}\frac{x}{\text{Sin}\theta_b}\right]_{-\text{Sin}\theta_b}^{\text{Sin}\theta_b} + \alpha\left[-\frac{x}{2}\ \text{Sin}^2\theta_b-x^2\right.$$

$$\left. + \frac{\text{Sin}^2\theta_b}{2}\text{Sin}^{-1}\frac{x}{\text{Sin}\theta_b}\right]_{-\text{Sin}\theta_b}^{\text{Sin}\theta_b}$$

$$= \pi(1+\frac{\alpha}{2}\ \text{Sin}^2\theta_b)$$

REFERENCES

1. N.A. Perifilov, Yu.F. Romanov and Z.I. Solove'va, Soviet Phys.- Uspekhi 3, 542 (1961).

2. S.W. Cosper, J. Cerny and R.C. Gatti, Phys.Rev. 154, 1193 (1967)

3. R. Ramanna, K.G. Nair and S.S. Kapoor, Phys. Rev. 129, 1350 (1963)

4. A Gillet, T.P. Doan, C. Carles and R. Chastel, C.R. Acad. Sc. Paris 262, 296 (1966)

5. R.A. Atneosen, T.D. Thomas and G.T. Garvey, Phys. Rev. 139, B 307 (1965)

6. V.A. Hattangadi, T. Methasiri, D.M. Nadkarni, R. Ramanna and P.N. Rama Rao in Physics and Chemistry of Fission (International Atomic Energy Agency, Vienna, 1965) Vol. II, P.397.

7. B.A. Bochagov, A.A. Vorobev and A.P. Komar, Sov. Phys. Tech. Physics. 2, 1458 (1957)

8. I. Ogawa, T.Doke and M.T. Sukuda, Nucl. Inst. and Methods 13, 169 (1961)

9. S.S. Kapoor, R. Ramanna and P.N. Rama Rao, Phys. Rev. 131, 283 (1963).

10. J.C.D.Milton and J.S. Fraser, Can. Jr.Phys. 40, 1626 (1962)

11. J.E. Simmons and R.L. Henkel, Phys. Rev. 120, 198 (1960)

12. V.G. Nesterov, G.N. Smirenkin and D.L. Shpak, Sov. Jr.Nucl. Physics. 4, 713 (1967)

13. A. Bohr, Proc.Int. Conf. on Peaceful Uses of Atomic Energy United Nations, New York (1956), Vol.2,p. 151.

14. N.A. Perfilov and Z.I. Soloveva, Sov.Phys. JETP 10 , 824 (1960)

15. I.Halpern in Physics and Chemistry of Fission International Atomic Energy, Vienna, 1965) Vol.II, p. 369

16. N. Feather, Proc. Roy: Soc. Edin. 66A, 192 (1964)

17. J.A. Coleman, A.W. Fairhall and I.Halpern, Phys. Rev. 133, B 724(1964)

18. T.D. Thomas and S.L. Whetstone, Phys. Rev. 144, 1060 (1966)

19. R.A. Nobles, Phys. Rev. 126, 1508 (1962).

20. A.W. Fairhall, I.Halpern and E.J. Winhold, Phys. Rev. 94, 733 (1954).
B.L. Cohen, W.H. Jones, G.H. McCormick, and B.L. Ferrell, Phys. Rev. 94, 625 (1954); A.N. Protopopov and O.P. Eismont. Atomnaya Energiya, 6, 644 (1959); J.A. Coleman, University of Washington Report (1962); S.S. Kapoor, D.M. Nadkarni, R. Ramanna and P.N. Rama Rao, Phys. Rev. 137, B 511 (1965).

21. V.N. Dmitriev, L.V. Drapchinskii, K.A. Petrzhak and Y.F. Romanov Sov. Phys. JETP 12, 390 (1961).

22. H.W. Schmitt, J.H. Neiler, F.J. Walter and A. Chetham-Strode, Phys. Rev. Letts. 9, 427 (1962).

FIGURE CAPTIONS

Fig.1. Schematic diagram of the ionization chamber and CsI crystal set up used in the first method.

Fig.2. The grid pulse height distribution for binary and ternary fission fragments in thermal neutron induced fission of U^{235}. The rectangular distributions shown by solid curves are the theoretical grid pulse height distributions obtained by dividing the selected energy region into 5 intervals. The superposition of these rectangular distributions is shown by the continuous dashed curve. $V(\Theta 1)$ and $V(\Theta 2)$ indicate the channel widths with equal solid angles in 0^o and 90^o regions.

Fig.3. The grid pulse height distribution for binary and ternary fragments in 3 MeV neutron fission of U^{235}. $V(\Theta 1)$ and $V(\Theta 2)$ indicate the channel widths giving equal solid angles in 0^o and 90^o regions.

Fig.4. Schematic diagram of the detector systems used in the second method. Semiconductor detectors D1, D2 and D3 were used to detect LRA, fragments emitted at 0^o and fragments emitted at 90^o with respect to incident neutron detection, respectively.

Fig.5. Schematic diagram of electronics used. The symbols have the following significance: PREAMP- preamplifier, AMP-amplifier, COINC-coincidence circuit, ANTI- COINC- anticoincidence circuit, DISC- discriminator, LG- linear gate, TRIG- trigger pulse.

Fig.6. Fragment pulse height distribution from D2 in 3 MeV neutron induced binary and ternary fission of U^{235}.

Fig.7. Fragment pulse height distribution from D3 in 3 MeV neutron induced binary and ternary fission of U^{235}.

Fig.8. Fragment pulse height distribution from D2 in thermal neutron induced binary and ternary fission of U^{235}.

Fig.9. Fragment pulse height distribution from D3 in thermal neutron induced binary and ternary fission of U^{235}.

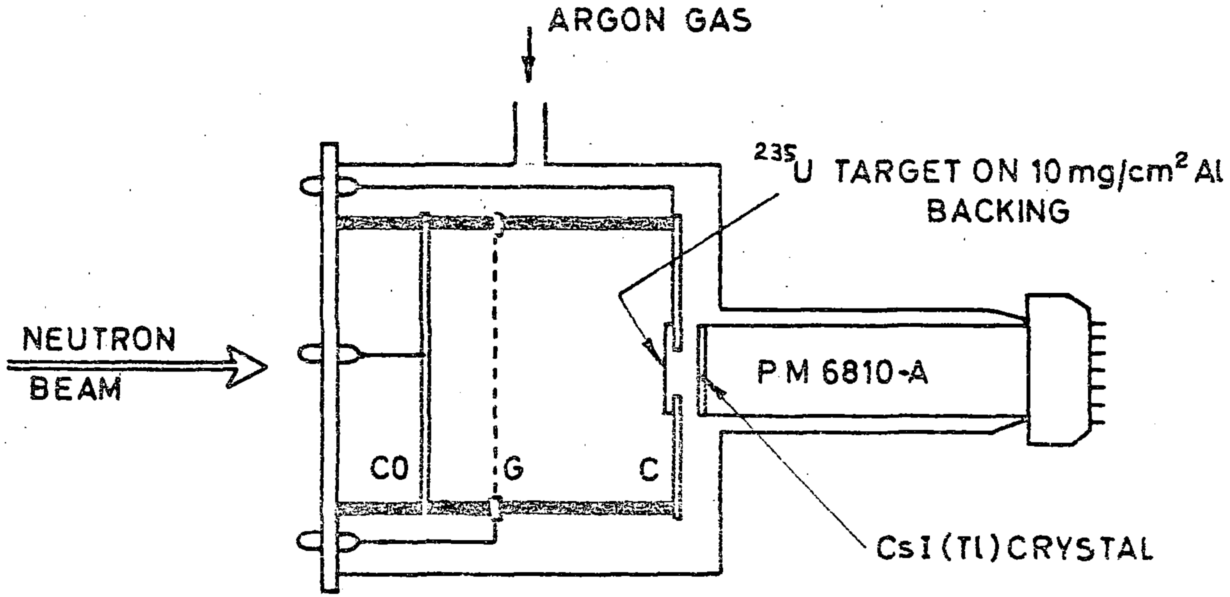
ARGON GAS
^{235}U TARGET ON 10 mg/cm^2 Al
BACKING
NEUTRON
BEAM
P M 6810-A
C0
G
C
CsI (Tl) CRYSTAL

FIG - 1

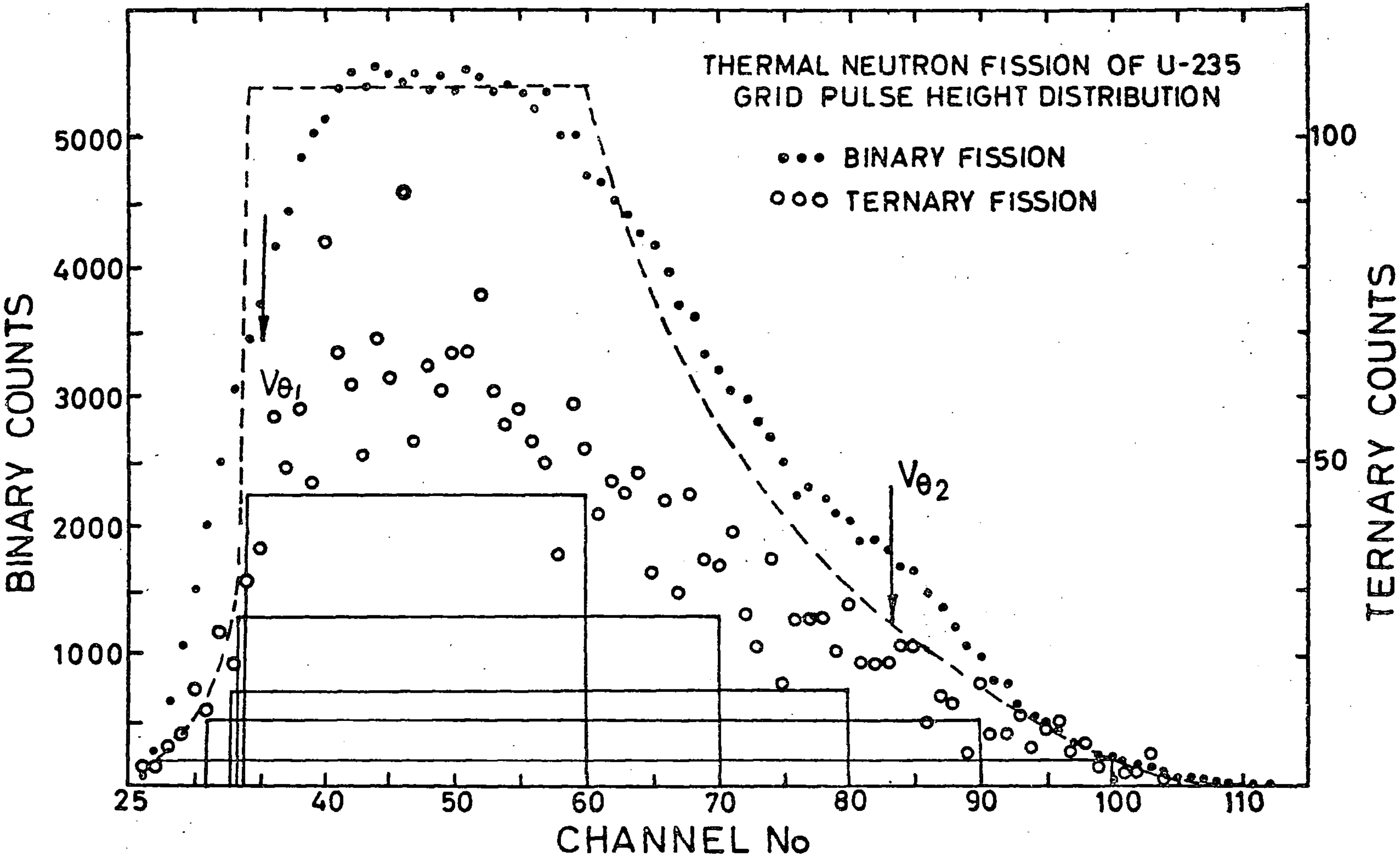
THERMAL NEUTRON FISSION OF U-235
GRID PULSE HEIGHT DISTRIBUTION
BINARY FISSION
TERNARY FISSION
BINARY COUNTS
TERNARY COUNTS
5000
4000
3000
2000
1000
100
50
25
40
50
60
70
80
90
100
110
CHANNEL No
Vθ1
Vθ2

FIG-2

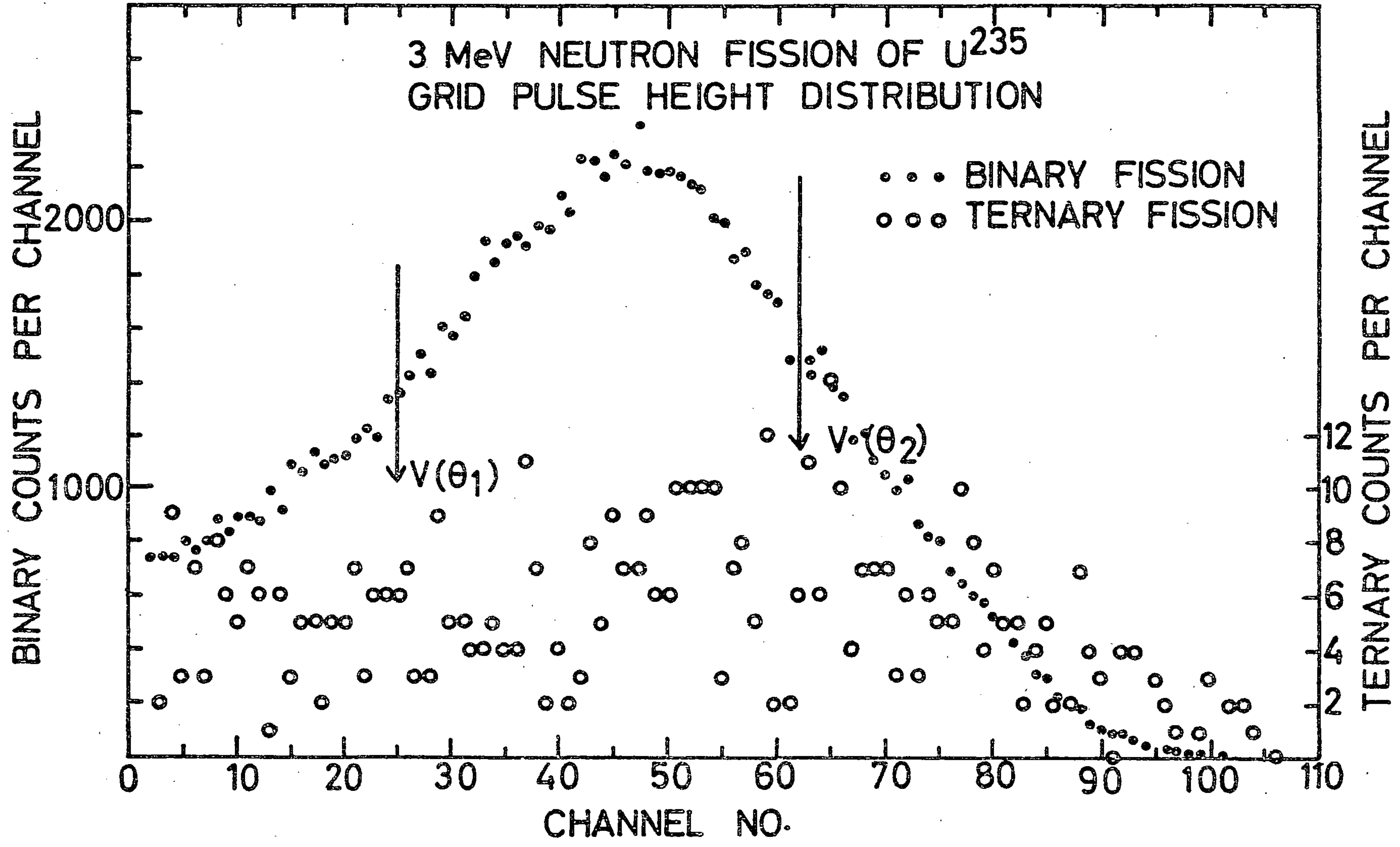
3 MeV NEUTRON FISSION OF U235
GRID PULSE HEIGHT DISTRIBUTION
BINARY FISSION
TERNARY FISSION
V(θ1)
V(θ2)
BINARY COUNTS PER CHANNEL
1000
2000
TERNARY COUNTS PER CHANNEL
2
4
6
8
10
12
CHANNEL NO.
0
10
20
30
40
50
60
70
80
90
100
110

FIG-3

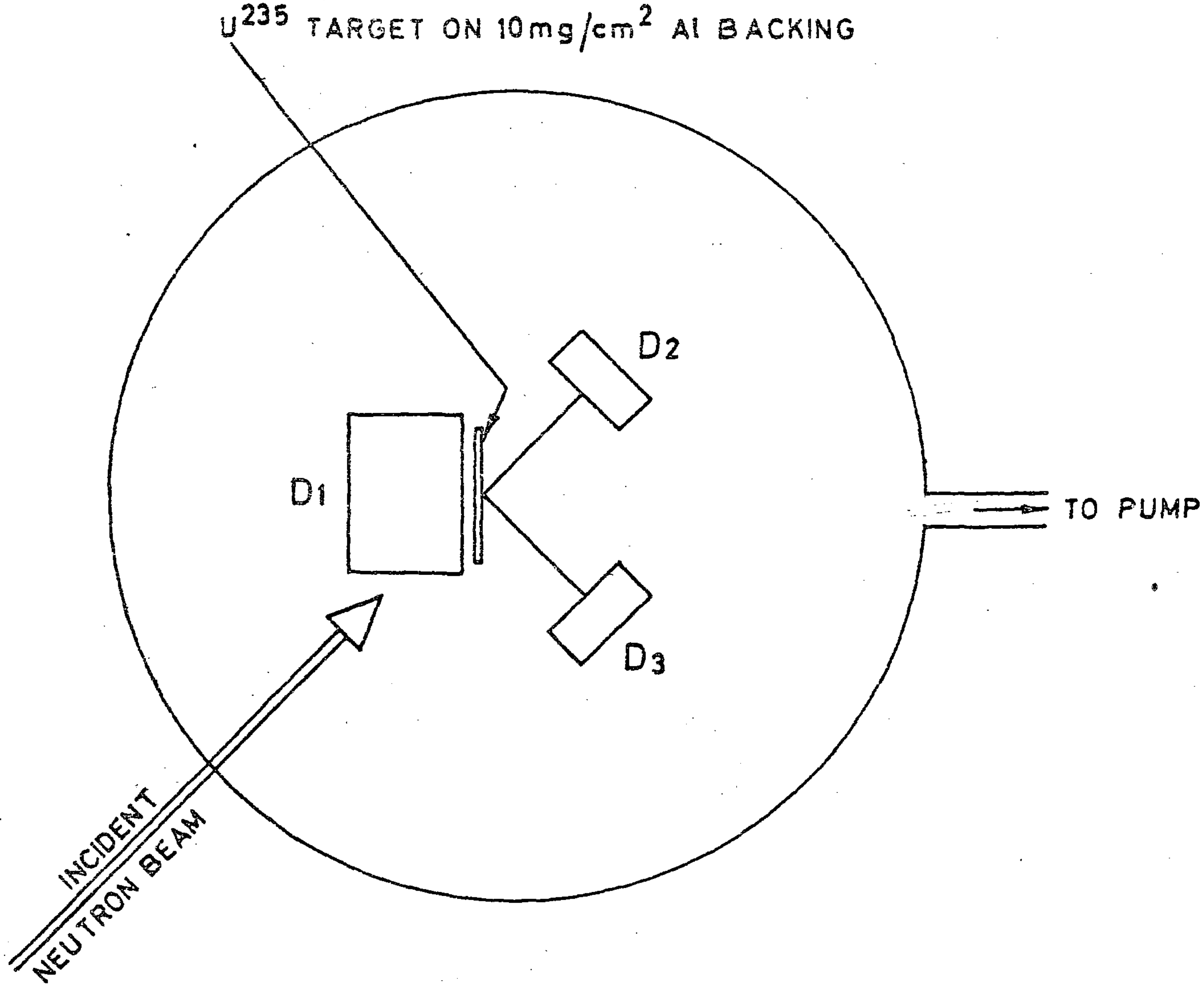
U235 TARGET ON 10mg/cm2 Al BACKING
D2
D1
D3
TO PUMP
INCIDENT
NEUTRON BEAM

FIG-4

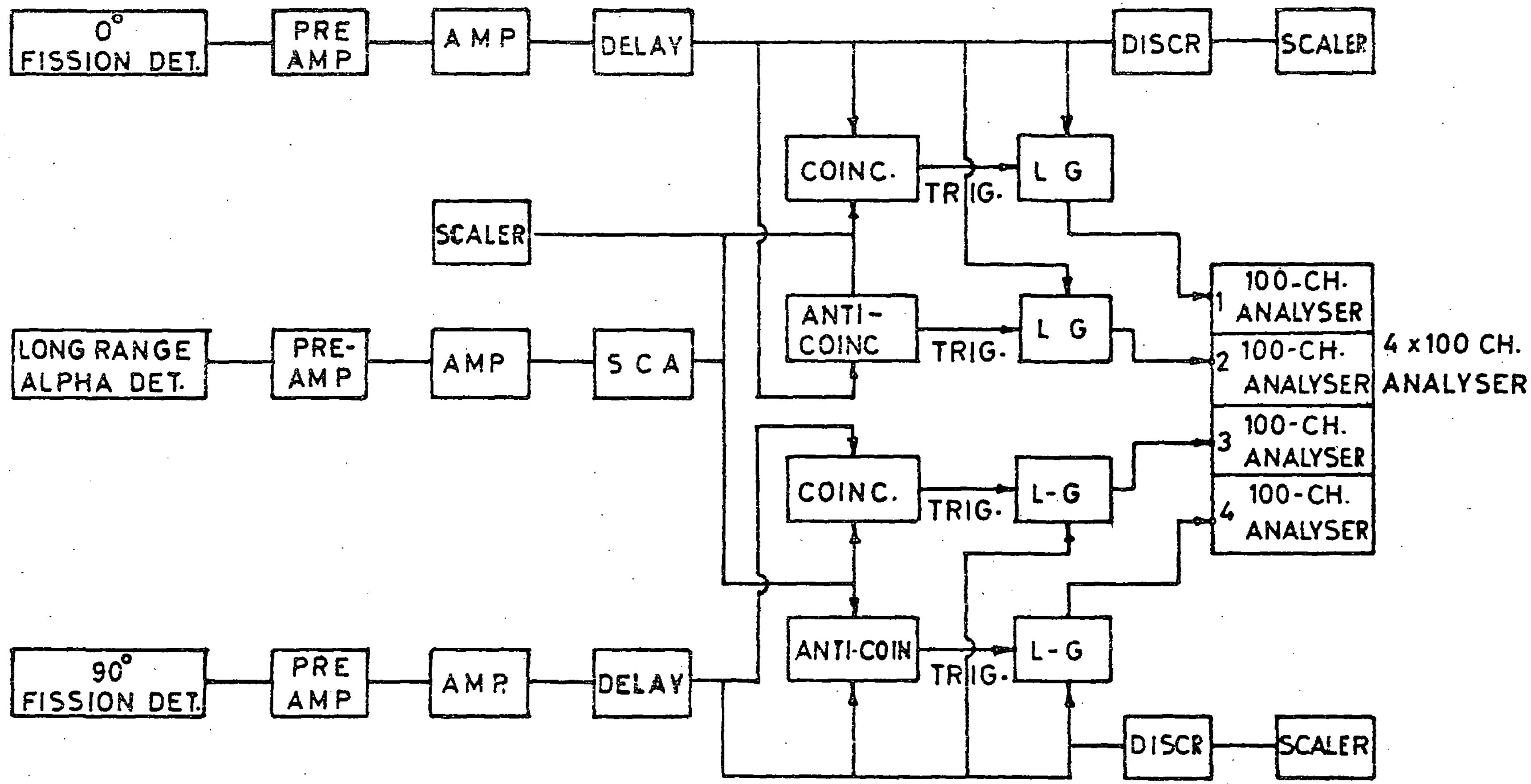

SCHEMATIC DRAWING OF ELECTRONICS

FIG-5

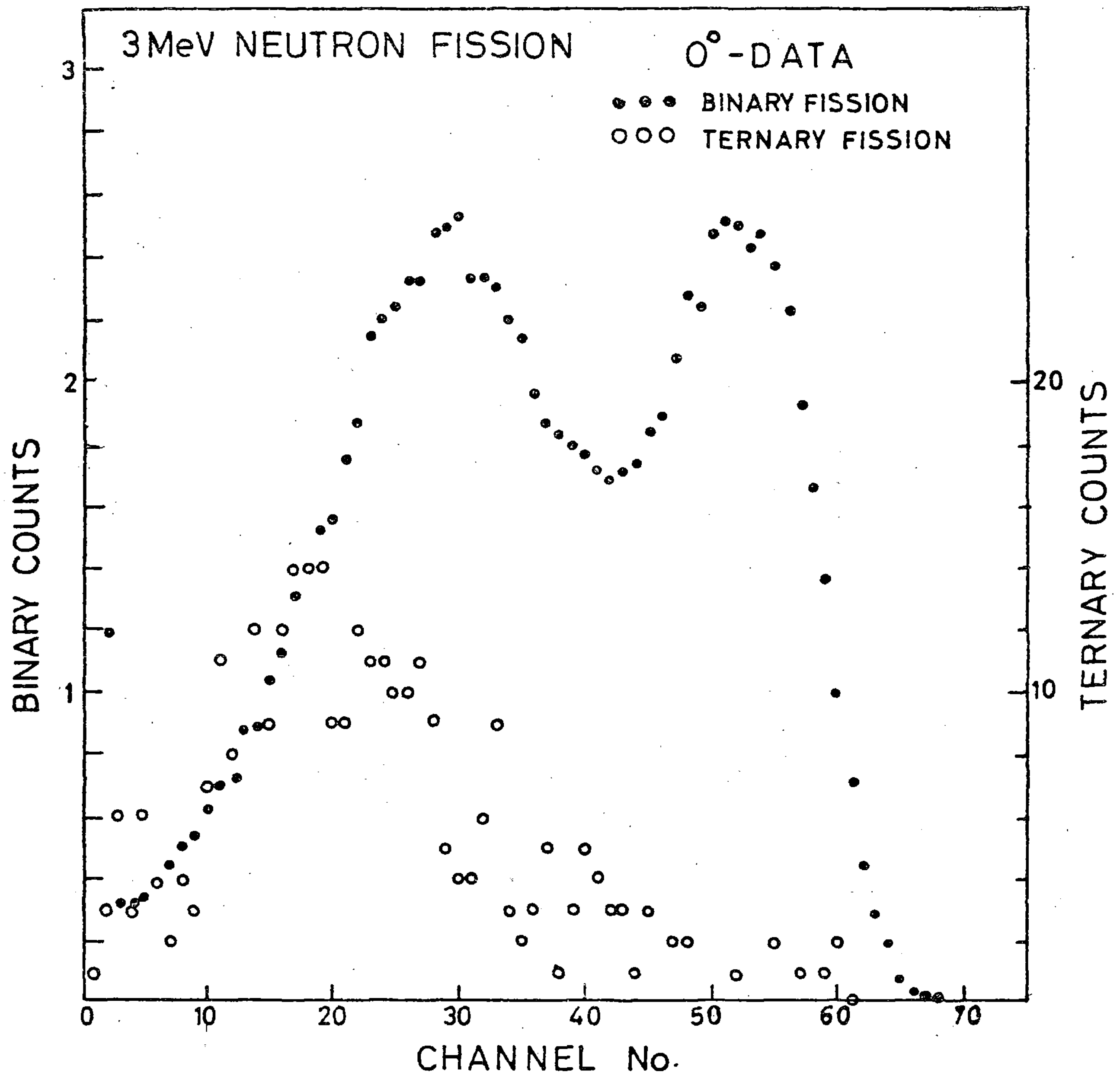
3MeV NEUTRON FISSION
0°-DATA
BINARY FISSION
TERNARY FISSION
BINARY COUNTS
TERNARY COUNTS
CHANNEL No.
3
2
1
20
10
0
10
20
30
40
50
60
70

FIG-6

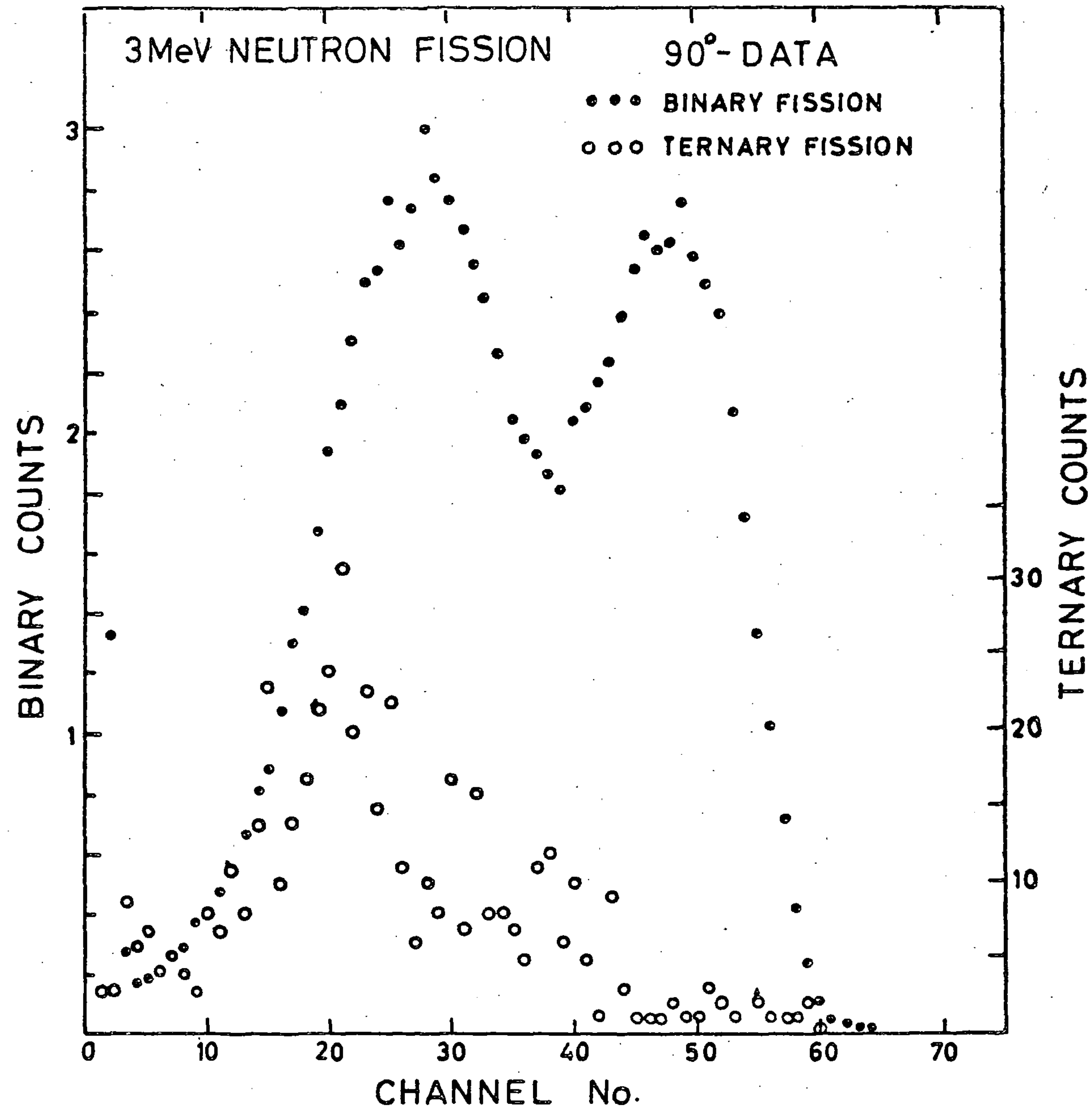
3MeV NEUTRON FISSION
90°- DATA
BINARY FISSION
TERNARY FISSION
BINARY COUNTS
TERNARY COUNTS
CHANNEL No.
0
10
20
30
40
50
60
70
1
2
3
10
20
30

FIG-7

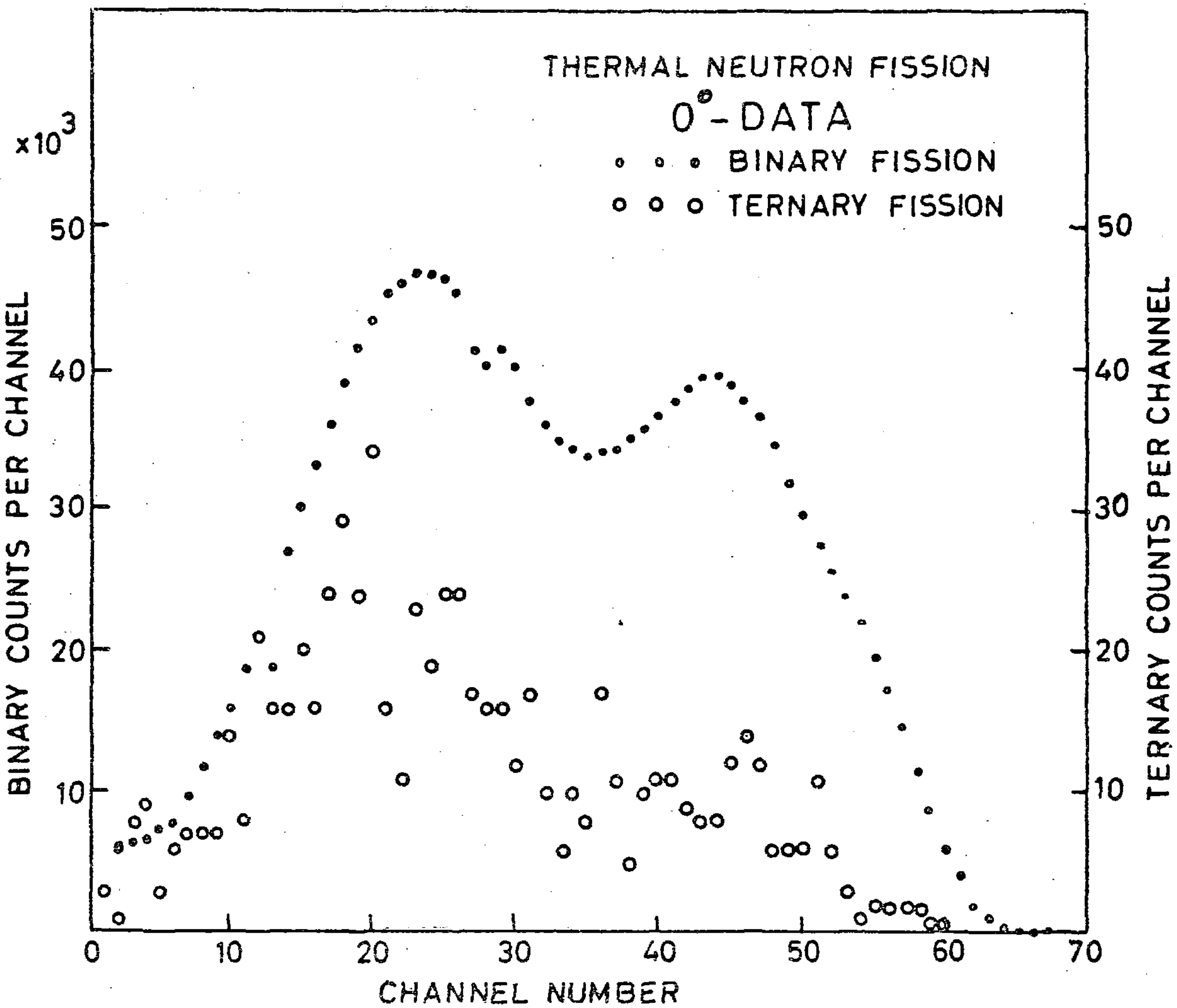
THERMAL NEUTRON FISSION
0°-DATA
BINARY FISSION
TERNARY FISSION
x10^3
50
40
30
20
10
BINARY COUNTS PER CHANNEL
TERNARY COUNTS PER CHANNEL
0
10
20
30
40
50
60
70
CHANNEL NUMBER

FIG-8

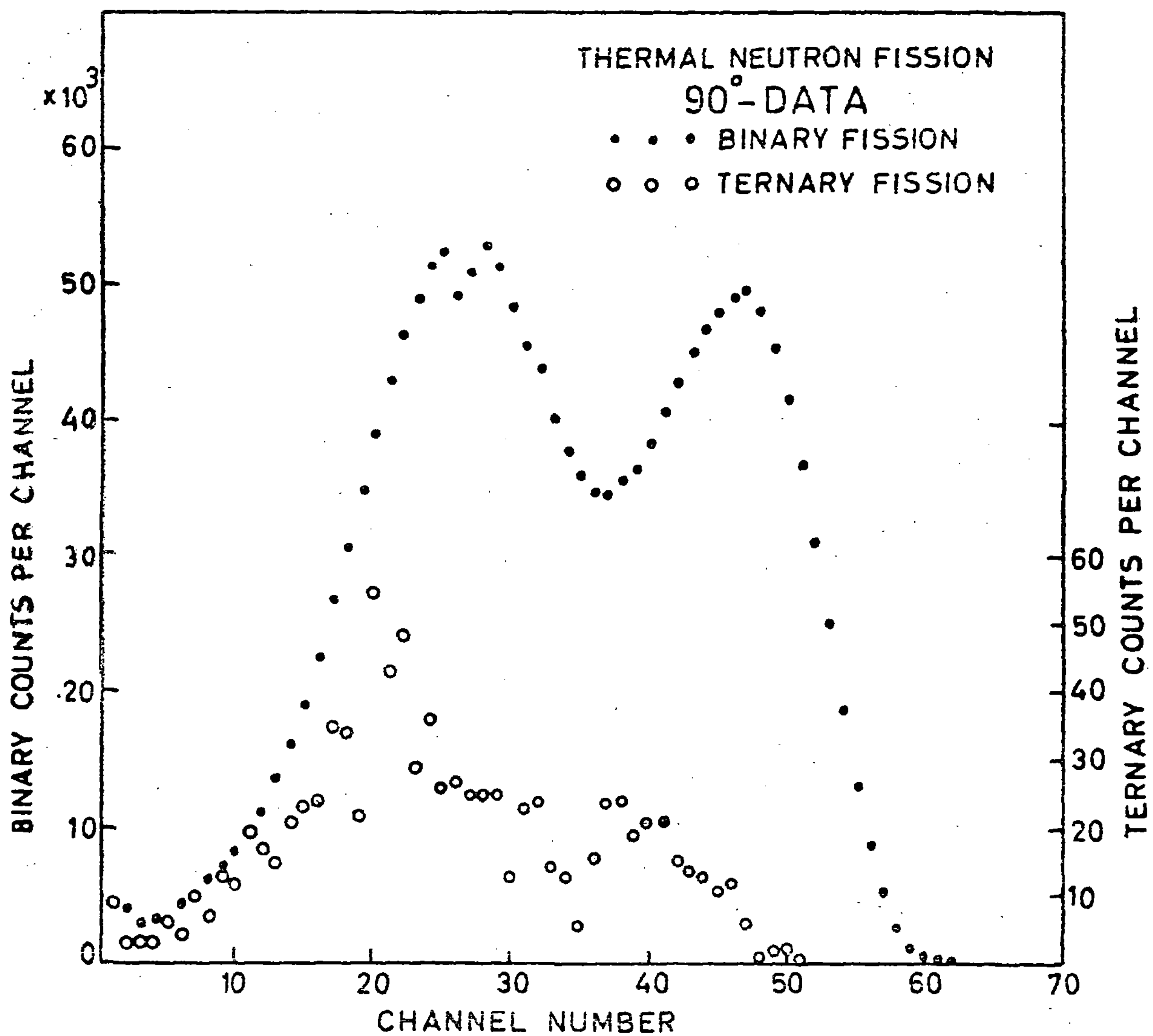
THERMAL NEUTRON FISSION
90°-DATA
BINARY FISSION
TERNARY FISSION
x10^3
BINARY COUNTS PER CHANNEL
TERNARY COUNTS PER CHANNEL
CHANNEL NUMBER

FIG-9